

Radial Harmonic Fourier Moments for CT-based Quantitative Radiomics*

A. H. M. Sajedul Hoque^{ab}, Gergő Bognár^{ac}, and Sándor Fridli^{ad}

Abstract

Radiomics is an emerging field of CT image processing, that offers non-invasive quantification of tumour phenotypes using quantitative image features. Radiomics analysis has promising applications in cancer treatment and personalized medicine, like treatment planning and the prediction of clinical factors. However, the optimal feature selection is not established in the literature, and the applications usually involve data mining of a large pool of features. In this paper, we propose to extract higher-level radiomic features using Radial Harmonic Fourier moments (RHF_M). Image moments, and specially orthogonal Fourier moments are widely used in image processing, providing efficient and invariant shape descriptors. In particular, RHF_Ms are known to perform well on small noisy images, making them a promising candidate for CT tumour analysis. Motivated by these advantages, we developed a feature extraction scheme based on RHF_M, and we performed radiomics analysis on lung CT images of non-small cell lung cancer patients. The proposed method is validated on multiple annotated datasets following the literature guidelines, evaluating the accuracy, stability, reliability, and prognostic value of the proposed features. The results show better reliability and otherwise comparable performance compared to the state-of-the-art wavelet descriptors. Furthermore, Fourier moments provide higher level of flexibility and possible adaptivity compared to wavelets, and unlike wavelet features, RHF_M features are invariant of position, size and orientation in the tumor region.

Keywords: radiomics, lung CT, quantitative imaging, radial harmonics, orthogonal moments

*Project no. K146721 and TKP2021-NVA-29 have been implemented with the support provided by the Ministry of Culture and Innovation of Hungary from the National Research, Development and Innovation Fund, financed under the K.23 "OTKA" and the TKP2021-NVA funding schemes.

^aDepartment of Numerical Analysis, ELTE Eötvös Loránd University, Budapest, Hungary

^bE-mail: sajed@inf.elte.hu, ORCID: 0000-0001-8291-9990

^cE-mail: bognargergo@staff.elte.hu, ORCID: 0000-0001-7818-5760

^dE-mail: fridli@inf.elte.hu, ORCID: 0000-0003-3531-2576

1 Introduction

Medical imaging, especially X-ray computed tomography (CT), is a primary diagnostic tool of clinical oncology. CT, as an imaging modality, noninvasively quantifies the internal tissue density, that might help the localization and characterization of the tumour. CT imaging is routinely used in many areas of clinical oncology not only for diagnosis, but also for therapy planning and monitoring. In therapy planning, CT provides precise visualization of the geometric shape of the tumour and the normal tissue, which helps to determine the optimum radiation dose distribution in the tumour [13].

In this paper, we research quantitative imaging for lung CT motivated by personalized medicine. Personalized medicine is an emerging field that promises better patient care by taking the genetic differences of the tumour into account. In this personalized medicine, predictive and prognostic data factors coming from multimodal information including clinical, imaging, and molecular data are merged to forecast treatment outcomes [10]. However, the molecular characterization of cancer is challenging, and usually requires invasive approaches (biopsies and surgeries), which themselves may be limited if the tumour is heterogeneous. CT imaging is a promising supplementary tool to quantify tumour phenotypes [11]. As a noninvasive tool, imaging is feasible not only to support oncological diagnosis and treatment planning, but also for the long term monitor of the therapy outcomes over time. Radiomics [20] is a quantitative imaging approach that aims to extract robust image features to quantify the tumour phenotype. These radiomics features employ mathematical algorithms describing the intensity, shape, statistical, and textural properties of the tumour, usually involving a large number of features. The heterogeneity of tumour region due to its molecular characteristic expresses the texture, which holds the information about the structural arrangement of its surface and the relationship with the surrounding environment. It is already shown that radiomics correlate to tumour phenotypes [2], and can also be utilized to predict distant metastasis [4].

This research discusses radiomics features characterized by first, second and higher order statistics, with the main focus on higher order features. Briefly, first-order statistical features aims to describe the overall gray-level distribution of the tumour by quantifying the voxel intensity histogram in the tumour region. Second-order statistics are used to characterize the tumour texture using local histograms in the voxel neighborhoods. Meanwhile, higher order statistical features aims to quantify potential hidden patterns inside the tumour region, usually involving an image transformation method, like wavelets or Laplacian-of-Gaussian (LoG) pyramids [21]. Here, the desired transformation method provides a compact scale-space or frequency-space decomposition, is spatially localized, and is invariant of position, size and orientation in the tumour region. The most widely used wavelet transform (see e.g., [2]) are favored compared to other transformations (e.g., Fourier transform) because of its efficiency, its ability to provide both space and frequency (i.e., scale) representation, and its spatial localization property. However, wavelets are shift-variant and lack explainability, which might be undesired in medical applica-

tions, and which serves as a motivation of our research.

Image moments are widely used transformation-invariant feature descriptors [12], popular for pattern recognition, object representation, and feature extraction. In particular, orthogonal moments provide efficient and stable time-frequency decompositions, with the support for adaptivity and interpretability. In this paper, we focus on radial harmonic Fourier moments (RHFMs) [16], since they provide better numerical properties compared to several other moments, and even perform well on small images in a noisy environment. Compared to wavelets they also offer shift-invariance. Therefore, they seem promising for higher order analysis of CT tumour. We propose RHFm reconstructions for higher order radiomics feature extraction. The proposed model is developed and validated using multiple annotated lung CT datasets of non-small cell lung cancer (NSCLC) patients. The feature selection, and the optimization of the decomposition parameters are performed according to the analysis of the reconstruction accuracy. Finally, we evaluated the reliability, stability and prognostic power of the proposed features, that are crucial requirements in a clinical environment. Here, we followed the literature guidelines, and compared the proposed method to wavelet-based radiomics features [2].

The key contributions of this paper are highlighted as follows:

1. We designed higher order radiomics features based on RHFm reconstruction of CT images.
2. We performed an accuracy analysis to select features and to optimize the decomposition parameters (order and repetitions) of RHFm decomposition.
3. We explored and analyzed a total number of 456 RHFm-based radiomics features of the reconstructed CT image, and compared them with the same number of wavelet-based features.

The rest of this paper is organized into the five sections. "Related Works" overview the most relevant related literature results. In the "Materials and Methods" section, a summary of the utilized radiomics features, a short description of the lung CT datasets, and the basics radial harmonic Fourier moments are provided. Here, we also introduce proposed method and optimize our feature selection. The "Result and Discussion" section presents the outcomes of this work and analyzes the results in terms of reliability, stability and prognosis value. Finally, in the "Conclusion and Future Work" section, we give the concluding remarks with some future works.

2 Related Works

In this section, we briefly review the related literature of quantitative radiomics and orthogonal moments.

2.1 Quantitative radiomics

Quantitative radiomics became popular recently, since it has been shown that quantitative image features are related to tumour phenotypes, offering noninvasive approach to support cancer treatment. In [2], the authors proposed 440 high-order radiomics features based on the intensity, shape, texture and wavelet transform and analyzed those features in terms reliability, stability and prognostic power on the RIDER dataset. The author claimed that he found many radiomics features having prognostic power which were not addressed before. Another claim was that the selected features through stability and reliability analysis was more informative. Finally, the authors proposed a radiomics signature for making association with gene profiles and showed the signature represents the general prognostic tumour phenotype.

In [4], the authors worked on the extraction of 635 radiomics features based on intensity, shape, texture, LoG and wavelet-based features to predict distant metastasis (DM) for lung adenocarcinoma patients. The authors did the prognostic analysis on these feature over 182 patients. They showed that only 35 features are strongly prognostics for DM and twelve features are prognostics for survival. A standardized mathematical model for extracting radiomics features is felt in the clinical oncology. In [21], the authors developed a flexible open-source framework including a set of well-defined and tested mathematical models for easing the extraction of features from 3D or 2D medical image.

Tang et al. extracted 688 radiomics features based on the first-order statistics, shapes, texture and wavelet filters to build a classification model for hepatocellular carcinoma (HCC) patients [18]. In their work, they showed that the combined features extracted from original CT image and wavelet-filtered image increase the classification performance significantly to classify HCC and non-HCC patients. However, these high-order features are not shift-invariant which motivates us to move orthogonal moment-based features. These orthogonal moments are explained briefly in the next section.

2.2 Orthogonal moments

The characterization, evaluation and manipulation of visual information inside the CT image is a general problem in clinical oncology. The preferable representations extract features that are invariant of size, position and orientation of the CT image. Image moments (see e.g., [15]) provide potentially transformation-invariant descriptors that are desired properties for CT image quantization in order to achieve reliability and stability. Here, we overview some historical developments in this field.

In 1962, Hu introduced a non-orthogonal moment known as geometric moment for image description, and derived moment invariants based on algebraic invariance in rectangular coordinates for visual pattern and character recognition [7]. One disadvantage of this classic moment is that its invariants are restricted to second- and third- order moments only. In addition, low-order geometric moments provide

less information about image details, while high-order moments are sensitive to noise. These problems can be resolved by using circular and orthogonal moments.

In 1980, Teague proposed Zernike Moments (ZMs) as image descriptors which were constructed from a set of orthogonal Zernike circular polynomials over the unit circle [19]. The zero points of the ZMs are located in long radial distance from the origin. Thus, although the ZMs are rotation-invariant, its application for scale-invariant pattern recognition is challenging for small images. Then, Sheng and Shen explored orthogonal Fourier–Mellin moments (OFFMs) including generalized ZMs and orthogonalized complex moments [1] in 1994. The main advantage of OFFMs is that the zero points are uniformly distributed over the radial interval. For this reason, OFFMs have better performance than ZMs, providing better description of small images [17].

However, OFFMs have difficulties to describe the center of the image for higher order moments because they tend to be infinite in the origin. Ping and Sheng in 2002 solved the problem by proposing Chebyshev–Fourier moments (CHFMs) which used various orders of Chebyshev polynomials over radial interval [14]. The aforementioned orthogonal moments including ZMs, OFFMs and CHFMs are based on the radial polynomials which cause numerical instability at high order of moments and high time complexity to compute the corresponding moments. In order to address these problems, Ping et al. developed new orthogonal moments known as Radial Harmonic Fourier Moments (RHFMs) where triangular function is used as radial function [16]. RHFMs are shifting, scaling, rotation, and intensity invariant, and performs better compared to CHFMs in multiple aspects, like representation near the origin, the description of small images, and noise sensitivity. These aspect are also desired for feature extraction of CT tumours that motivated our choice.

3 Materials and Methods

In this section, we provide details of the theoretical and computational background, the validation datasets, and the proposed method.

3.1 Radiomics Features

In clinical oncology, radiomics features can used to monitor the development, progression of the cancer and the response to therapy. Those features are constructed employing advanced hand-coded algorithms, that provide a large set of quantitative imaging features. Aerts et al. [2] decomposed the CT image using wavelet decomposition and analyzed 440 radiomics features in order to build radiogenomics signature. These are experimental features, without detailed explanation. In [21], the authors developed a flexible open-source PyRadiomics platform for extracting features from medical image. This platform provides a set of very well-defined, tested and standardized mathematical models for radiomics features. Thus, we used these verified features to analyze in our study which are grouped under the following categories.

- **Shape and size related features** illustrates the three-dimensional size and shape of tumour region, using elementary geometric descriptors. The common features include elongation, flatness, least axis length, major axis length, maximum 2D diameter column, maximum 2D diameter row, maximum 2D diameter, mesh volume, minor axis length, sphericity, surface area, surface volume ratio, voxel volume. We note that these features are independent of the high-order decompositions discussed in this paper, so they are excluded from the analysis, and they are mentioned only for the sake of completeness.
- **First order statistical (FOS) features** describes the gray distribution in the tumour area by means of statistical properties of the image histogram. We considered 18 descriptors: 10th percentile, 90th percentile, energy, entropy, inter quartile range, kurtosis, maximum, mean absolute deviation, mean, median, minimum, range, robust mean absolute deviation, root mean squared, skewness, total energy, uniformity and variance.
- **Second order statistical features** illustrate the statistical correlation between a voxel and its neighboring voxels, addressing texture information. That is, second order features describe the heterogeneity of the tumour. In order to extract the texture features, matrices like Gray-Level Co-Occurrence Matrix (GLCM) and Gray-Level Run-Length Matrix (GLRLM) are formed from the CT image. GLCM provides the probability of combined occurrence of two intensity values. From that matrix, 24 features including autocorrelation, cluster prominence, cluster shade, cluster tendency, contrast, correlation, difference average, difference entropy, difference variance, inverse difference (ID), inverse difference moment (IDM), inverse difference moment normalized (IDMN), inverse difference normalized (IDN), informational measure of correlation 1 (IMC1), informational measure of correlation 2 (IMC2), inverse variance, joint average, joint energy, joint entropy, maximal correlation coefficient (MCC), maximum probability, sum average, sum entropy and sum square can be extracted. GLRLM represents the run-length of gray level in the CT image and the 16 associated GLRLM features are gray level non uniformity, gray level non uniformity normalized, gray level variance, high gray level run emphasize, long run emphasize, long run high gray level run emphasize, long run low gray level run emphasize, low gray level run emphasize, run entropy, run length non uniformity, run length non uniformity normalized, run percentage, run variance, short run emphasize, short run high gray level run emphasize and short run low gray level run emphasize.
- **High-order statistical features** aim to characterize repeated or nonrepetitive potential patterns inside the tumour region. For this purpose, images are decomposed using different scale-space transformations, like wavelets and Laplacian-of-Gaussian (LoG) pyramids. After the transformation, first and second-order statistical features are extracted from the decomposed images.

We also refer the reader to [20] for further information. In our work, as the the GLCM matrix is symmetrical, sum average feature under the GLCM category

is 2 times of joint average feature. So, the total number of first and second order statistical features is 57 (18+23+16). Higher-order statistical features are extracted from 8 decomposed images using wavelet decomposition and 8 order reconstructed images employing RHFMs. Therefore, we analyzed a total of 456 wavelet and the same number of RHFMs features in terms of reliability, stability and prognostic value.

3.2 Datasets and Data Analysis

In this study, three lung CT datasets are considered, involving non-small cell lung cancer (NSCLC) patients:

- **The RIDER test/retest dataset** [2] provides blind delineations to 32 patients of the RIDER Lung CT dataset where the delineations of three patients are not perfectly provided [22]. RIDER Lung CT consists of same day repeat scans, where two CT scans were acquired from each patient within 15 minutes. In this study, this dataset is used to assess the reliability of the features.
- **The multiple delineation dataset** [2] consists of lung CT scans of 21 patients which were manually delineated by five oncologists independently. As one patient has no manual delineation, twenty CT images of patients are used to assess the feature stability.
- **The Lung1 dataset** [2] consists of lung CT scans of 422 patients, together with manual delineations, clinical, survival data and gene profiles. It has been observed that three out of 422 patients have absent of proper masks. Thus, the radiomics features are extracted from 419 patients. This dataset is used to assess the prognostic value of the radiomic features.

3.3 Image Reconstruction using RHFm

In this study, we propose to extract higher order radiomic features based on RHFm reconstruction. The theoretical background, and the RHFm decomposition and reconstruction method are described below.

3.3.1 Radial Harmonic Fourier Moments

Following [16], consider the radial harmonic basis function H_{pq} ($p \in \mathbb{N}$, $q \in \mathbb{Z}$), defined in polar coordinates as

$$H_{pq}(r, \varphi) := R_p(r)e^{iq\varphi} \quad (r \in [0, 1], \varphi \in [0, 2\pi)), \quad (1)$$

where

$$R_p(r) := \begin{cases} 1/\sqrt{r}, & \text{if } p = 0, \\ \sqrt{2/r} \cos(\pi pr), & \text{if } p \text{ is even,} \\ \sqrt{2/r} \sin(\pi(p+1)r), & \text{if } p \text{ is odd.} \end{cases}$$

Radial harmonic basis functions form a complete orthonormal system in the space of the square integrable functions over the unit disk (i.e., in $L^2(\mathbb{D})$) with respect to the usual scalar product

$$\langle F, G \rangle := \frac{1}{2\pi} \int_0^{2\pi} \int_0^1 F(r, \varphi) G^*(r, \varphi) r dr d\varphi \quad (F, G \in L^2(\mathbb{D})). \quad (2)$$

A grayscale image, represented as a function $f \in L^2(\mathbb{D})$ over the unit disk, can be decomposed into a series expansion as

$$f(r, \varphi) = \sum_{p=0}^{+\infty} \sum_{q=-\infty}^{+\infty} M_{pq} H_{pq}(r, \varphi) \quad (r \in [0, 1], \varphi \in [0, 2\pi)),$$

where

$$M_{pq} := \langle f, H_{pq} \rangle = \frac{1}{2\pi} \int_0^{2\pi} \int_0^1 f(r, \varphi) H_{pq}^*(r, \varphi) r dr d\varphi$$

is the radial harmonic Fourier moment (RHF_M) of order $p \in \mathbb{N}$ and repetition $q \in \mathbb{Z}$.

3.3.2 Image Decomposition

The real application of RHF_Ms involves discretization and the restriction of the input image to the unit disk. Here, we followed the discretization and numerical integral approximation proposed in [3]. Normally, planar images are organized as the matrix of pixels over rectangular coordinate system, where the coordinate of the left top corner pixel is $(0, 0)$. Consider a grayscale image $f(x, y)$, and assume that it is square of size $N \times N$. As the RHF_M is based on the polar coordinate system, an inner unit circle is inscribed over the grayscale image. Then, the origin of the image is moved to the center of the inscribed circle, and the central coordinate of all pixels of the input image $f(x_i, y_j)$ are computed as

$$x_i = \frac{2j - N + 1}{N}, \quad y_j = \frac{N - 1 - 2i}{N} \quad (i, j = 0, 1, 2, \dots, N - 1). \quad (3)$$

After mapping, the new Cartesian coordinates (x_i, y_j) over the inscribed inner circle are transformed into the polar coordinate (r_{ij}, θ_{ij}) as

$$r_{ij} = \sqrt{x_i^2 + y_j^2}, \quad \theta_{ij} = \text{atan2}(y_j, x_i) \quad (i, j = 0, 1, 2, \dots, N - 1), \quad (4)$$

where $\text{atan2}(y, x) = \arg(x + iy)$ denotes the two-argument arctangent. The RHF_Ms M_{pq} of the image $f(r_{ij}, \theta_{ij})$ with order $p \in \mathbb{N}$ and repetition $q \in \mathbb{Z}$ over a unit inner circle are computed employing the discrete representation of (2) as of

$$M_{pq} = \frac{2}{\pi N^2} \sum_{i=0}^{N-1} \sum_{j=0}^{N-1} f(r_{ij}, \theta_{ij}) H_{pq}^*(r_{ij}, \theta_{ij}). \quad (5)$$

Note that the radial factor in (1) depends on the radius of the pixel located in (x_i, y_j) coordinate and the order p of that radius, and the exponential factor relies on the angular distance from x-axis of the pixel and its repetition q . Assuming that the maximal order and repetition of the computed moments are $p_{max} \in \mathbb{N}$ and $q_{max} \in \mathbb{Z}$, respectively, the total number of RHFMs is $(1 + p_{max}) \times (1 + 2q_{max})$.

3.3.3 Image Reconstruction

In this paper, we extract radiomics features using low-level reconstructions using RHFMs. To this order, consider the partial reconstruction of order $p_{max} \in \mathbb{N}$ and repetition $q_{max} \in \mathbb{Z}$ as

$$f(r, \varphi) \approx \hat{f}(r, \varphi) := \sum_{p=0}^{p_{max}} \sum_{q=-q_{max}}^{q_{max}} M_{pq} H_{pq}(r, \varphi) \quad (r \in [0, 1], \varphi \in [0, 2\pi)). \quad (6)$$

The reconstructions represent low-dimensional approximations of the input image based on the transformation-invariant moment decomposition.

3.4 Proposed Method

Based on the above motivations and background information, we propose RHFm reconstructions for high-order radiomic feature extraction. Orthogonal moments provide efficient frequency-space representations that can capture high-level patterns on the image, and have further beneficial properties like transformation-invariance. These make them promising replacements of the wavelet-based high-order features suggested in [2] and [21]. In particular, RHFMs show better numerical stability compared to other constructions, and perform well for small noisy images, desired for CT tumour images. In the following, we summarize the proposed algorithms, and provide further insight and justification.

3.4.1 Image Representation

The key part of the proposed method is the representation of the CT tumour image using RHFm. The overall steps are summarized in the Algorithm 1. The algorithm takes four inputs: the 3D CT image (I), its 3D mask (M), and the maximal order (p) and repetition (q) for RHFm decomposition and reconstruction; and returns the reconstructed image based on the RHFm representation.

We note that the representation is performed on the raw CT images without any filtering or resampling. The only preprocessing step is the correction, cropping, and squaring the CT image and tumour mask in order to handle the inconsistencies of the target databases regarding pixel size, spacing, and origin. A sample of cropped CT tumour image is shown in Fig. 1.

3.4.2 Feature Selection

In the next phase, we optimized feature selection, where we investigated the optimal parameters of RHFm decomposition and reconstruction. To this order, we

Algorithm 1 Proposed Algorithm for Image Representation using RHF_M.

Funct RECON(I, M, p, q)

- 1: Remove inconsistency by correcting, cropping and squaring the image I and the mask M with $N \times N$ size of each slice
 - 2: Combine the 3D image I and the mask M into a new 3D image C
 - 3: Shift the intensity range of the image C to $[0, \text{range of intensity}]$
 - 4: Map each Cartesian coordinate (x, y) into the central coordinate (x_i, y_j) over inscribed circle as of (3) and compute the polar coordinate (r_{ij}, θ_{ij})
 - 5: Select the list of orders $P = [0, 1, \dots, p]$ and the list of repetitions $Q = [-q, -q + 1, \dots, q - 1, q]$
 - 6: Compute the radial harmonic basis functions $H_{pq}(r_{ij}, \theta_{ij})$ being a matrix of size $((p + 1) \times (2q + 1) \times N \times N)$, where p and q is an order and repetition from P and Q , respectively
 - 7: Setup the output array \hat{C} as shape of image C
 - 8: **for** each slice $f(x, y)$ in C **do**
 - 9: Compute matrix of moments M_{pq} of size $((p + 1) \times (2q + 1))$ by performing the inner product of the image $f(x, y)$ and the radial harmonic basis function $H_{pq}(r_{ij}, \theta_{ij})$ as of (5)
 - 10: Compute the reconstructed slice $\hat{f}(x, y)$ by the partial sum of radial harmonic basis functions $H_{pq}(r_{ij}, \theta_{ij})$ weighted by moments M_{pq} as of (6)
 - 11: Store the reconstructed slice $\hat{f}(x, y)$ in \hat{C}
 - 12: **end for**
 - 13: Clip and shift back the intensity of image \hat{C} over the range of image C
 - 14: **return** the reconstructed image \hat{C}
-

evaluated the error in terms of mean squared reconstruction error of the form

$$MSRE = \frac{\sum_{x=0}^{N-1} \sum_{y=0}^{N-1} |f(x, y) - \hat{f}(x, y)|^2}{\sum_{x=0}^{N-1} \sum_{y=0}^{N-1} |f(x, y)|^2}. \quad (7)$$

Fig. 2, 3, and 4 present the average MSRE of the three datasets. In this evaluation, we set the order and repetition of RHF_M to be the same, i.e., $p = q$, as of [16]. Furthermore, we investigated even orders only in order to include both the sine and cosine radial functions of the same magnitude. The analysis show that the representation is optimal around order 10, which behaviour is following the theoretical expectations: when the order is too low, then the error is high due to the loss of detail information on the image, and when the level is too high, then numerical errors arise due to noise and discretization artifacts. In conclusion, we propose to select the eight orders around 10 for CT image representation, namely we suggest the list of [2, 4, 6, 8, 10, 12, 14, 16].

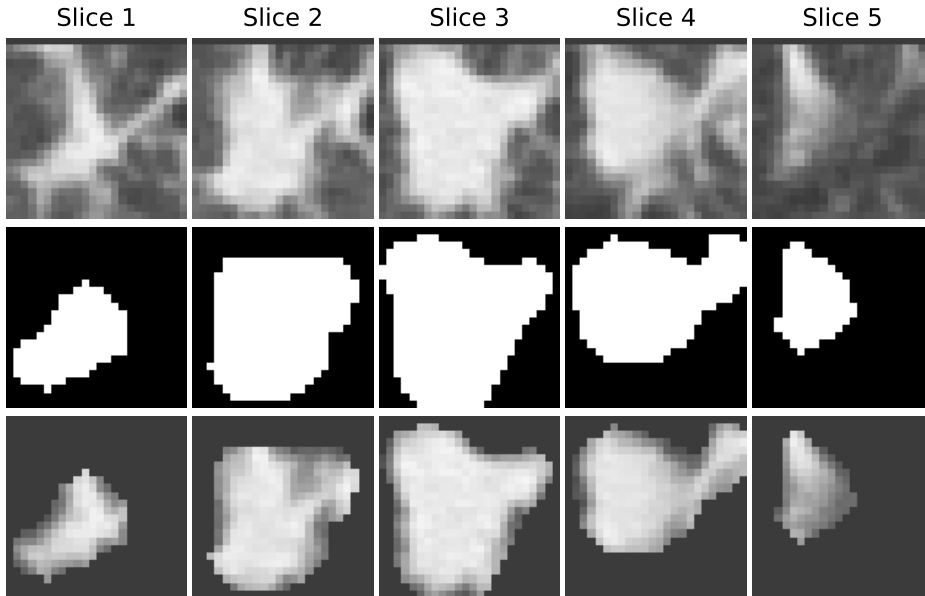


Figure 1: A sample of preprocessed CT Image of Lung1 Dataset. Rows: original CT slices (cropped, squared), tumour masks, and masked tumour images.

3.4.3 Feature Extraction

We propose radiomics feature extraction following the methodology of [2], and utilizing the lower-order features of [21]. There, one step of 3D stationary wavelet decomposition was utilized using Coiflet 1, resulting eight image representations for high-order feature extraction. Instead, we propose eight RHFMs reconstructions here in the above manner. Then, 18 first-order statistical, 23 GLCM and 6 GLRLM-related features are extracted from those reconstructed images, as introduced above. Totally, we investigated 456 RHFMs-based features, which we compared to the same amount of wavelet-based features as of [2]. The low-order features were extracted using the pyradiomics package [21].

As a comparison, the eight wavelet decompositions of the CT image shown in Fig. 1 are illustrated in Fig. 5 and 6, and eight RHFMs reconstructions are shown in Fig. 7 and 8.

4 Results and Discussion

In this study, the extracted 456 radiomics features of lung cancer are analyzed to evaluate their reliability, stability, and prognostic power, following the workflow proposed in [2]. For this reason, statistical tests are applied to determine scores

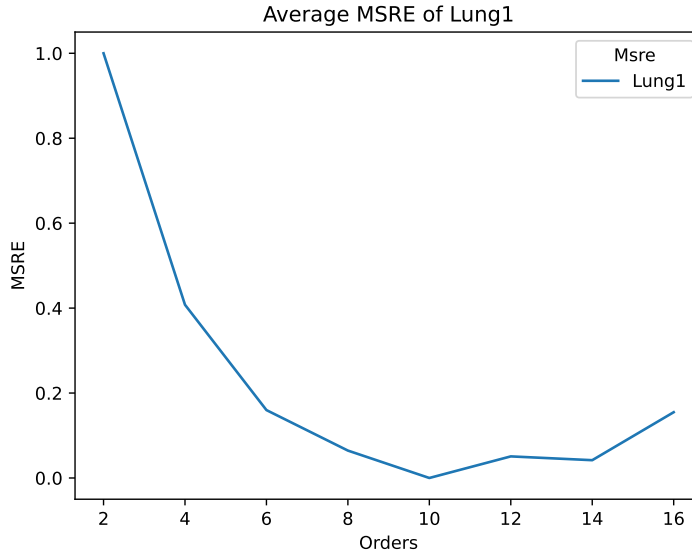


Figure 2: Average MSRE of Lung1 Dataset

for the reliability, stability and prognostic value of those extracted features. We explain and evaluate the score below, and compare the proposed method to the wavelet-based approach in [2].

4.1 Reliability Analysis

In conservative medicine, the reliability of numerical measurements of patients are always intended to evaluate for making decisions. Reliability implies the assessment of the reproducibility of the numerical measurements over the same set of patients. Thus, it emphasizes not only the correlation but also the agreement between measurements. Mathematically, reliability is the ratio of true variance over the true variance plus the error variance of measurements. The score of the reliability ranging from 0 to 1 can be evaluated by Pearson correlation coefficient, paired t -test and Bland-Altman plot. Those approaches are not ideal for reliability analysis, as Pearson correlation coefficient focus only on the correlation while paired t -test and Bland-Altman plot emphasize only on the agreement. Then, intraclass correlation coefficient (ICC) first introduced by Fisher in 1954 is widely used for reliability analysis. The ICC score representing both correlation and agreement between measurements is the index to quantify the reliability. The conservative care practitioners usually perform three types of reliability: interrater, intrarater and test-retest reliability. In interrater reliability, ICC score is based on the measurements taken by different raters over same patients, whereas same raters take measurements on same patients through one or more trial in intrarater reliability.

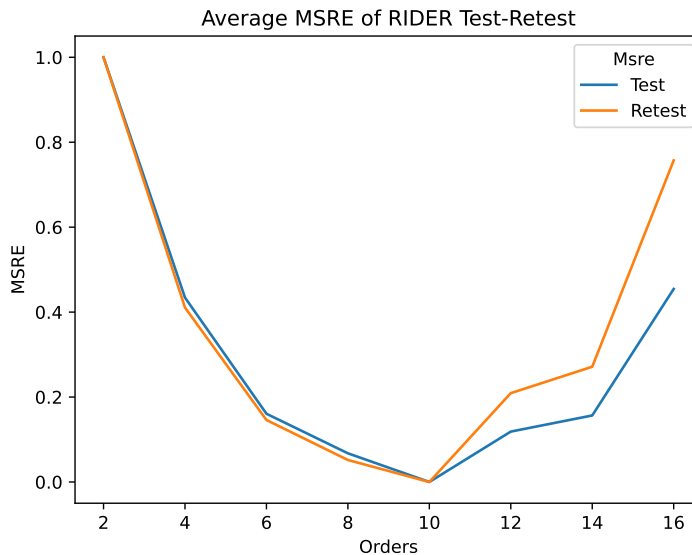


Figure 3: Average MSRE of Test-Retest Dataset

In the test-retest reliability, the measurements of the same subjects are taken by same instruments under same conditions at different time. In this study, the retest CT images of 31 subjects are taken after a 15 minutes tea break of taking the test CT image of the same patients in RIDER test-retest dataset. Therefore, the test-retest reliability is suitable for our study. There is no standard acceptable ICC value for reliability and the only expected value of ICC is the true ICC estimate. For this reason, the level of reliability is applied to determine for testing if the obtained ICC exceeds in statistical inference. Koo and Li suggested four levels of reliability in his guidelines for ICC reporting: Poor Reliability ($ICC < 0.5$), Moderate Reliability ($ICC \geq 0.5$ and $ICC < 0.75$), Good Reliability ($ICC \geq 0.75$ and $ICC < 0.9$) and Excellent Reliability ($ICC \geq 0.9$ and $ICC \leq 1$) [9]. This guideline for level of reliability has been used in this research where the ICC score of each feature is determined by employing intraclass correlation coefficient approach over two samples of each feature coming from test and retest CT scans. Table 1 shows the distribution of the number of RHFm and wavelet features among those groups (poor, moderate, good and excellent) to the usual guidelines. The table implies that the RHFm features show better reliability than wavelet features.

4.2 Stability Analysis

In clinical oncology, the tumor region of CT image of patients is delineated by multiple radiation oncologists for stability analysis. Multiple samples including desired extracted radiomics features from delineated CT images are compared to test if

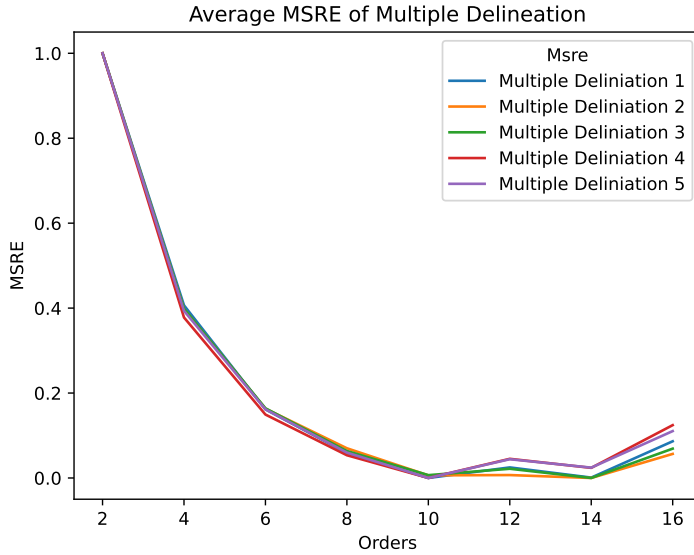
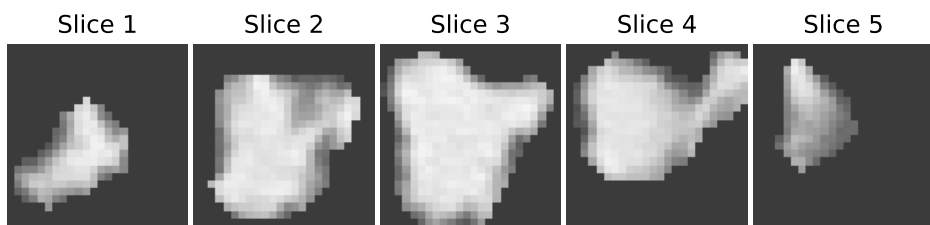


Figure 4: Average MSRE of Multiple Delineation Dataset

Table 1: Reliability: number of features based on ICC

Type of Features	Poor	Moderate	Good	Excellent
RHFM	22	105	175	154
Wavelet	38	89	157	172

there are any significant difference among the means of those samples. As those multiple samples are dependent, Repeated-Measures ANOVA and Friedman Test are used for the statistical test. As Repeated-Measures ANOVA test is parametric test, the assumptions of samples are to be normally distributed. If the assumptions of normality are not met, the Friedman test is used [5]. In this study, RIDER Multiple delineation data consisting of the CT scans of 21 patients delineated by five radiation oncologists are used to test stability. The Friedman test is applied over five samples of each feature avoiding the distribution of those sample. The test provides the p -value which is a probability that measures the evidence against the null hypothesis. That is, if the p -value of a feature is greater than the usual significance level of 5%, the feature is considered to be stable. Otherwise, the feature is not stable. It has revealed that there are 74 and 135 stable features for RHFMs reconstruction and wavelet decomposition, respectively, at a 5% significance level. The test shows that the RHFMs features and wavelet features are comparable in terms of stability.



(a) Original CT Image



(b) LLL Wavelet Image



(c) LLH Wavelet Image

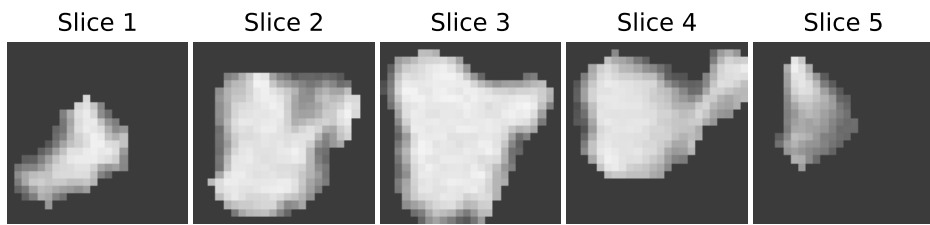


(d) LHL Wavelet Image



(e) LHH Wavelet Image

Figure 5: Wavelet Decomposed Images (LLL, LLH,LHL,LHH)



(a) Original CT Image



(b) HLL Wavelet Image



(c) HLH Wavelet Image

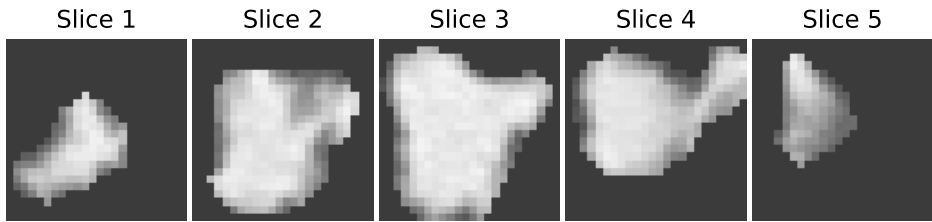


(d) HHL Wavelet Image

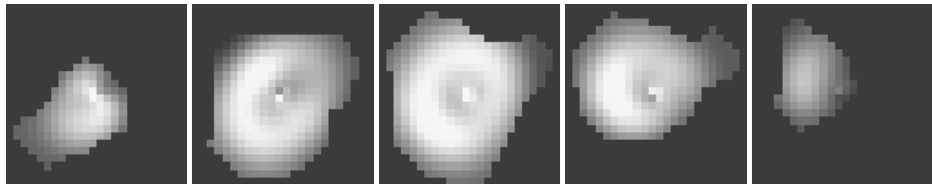


(e) HHH Wavelet Image

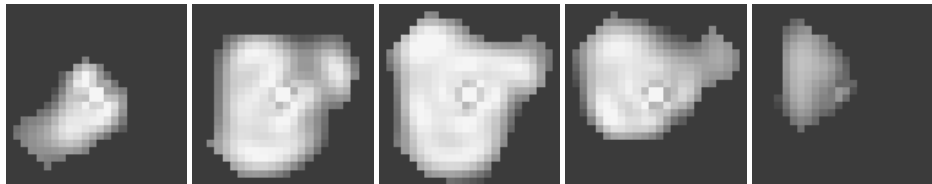
Figure 6: Wavelet Decomposed Images (HLL,HLH,HHL,HHH)



(a) Original CT Image



(b) Order 2 (MSRE: 0.163)



(c) Order 4 (MSRE: 0.072)

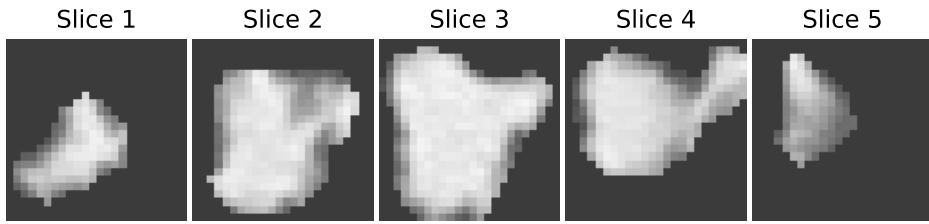


(d) Order 6 (MSRE: 0.057)

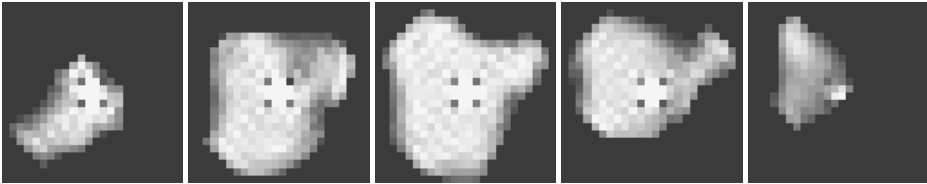


(e) Order 8 (MSRE: 0.055)

Figure 7: Reconstructed Images from RHFMs (order 2 to 8)



(a) Original CT Image



(b) Order 10 (MSRE: 0.058)



(c) Order 12 (MSRE: 0.061)



(d) Order 14 (MSRE: 0.071)



(e) Order 16 (MSRE: 0.086)

Figure 8: Reconstructed Images from RHFMs (order 10 to 16)

4.3 Prognosis Analysis

Generally, prognosis refers to the expected course and outcomes of a disease over time. In medical science, healthcare professionals make the assessment considering the likely course of a condition and its potential results based on their scientific knowledge, clinical experience and the circumstance of individual patient. This assessment helps the doctor to guide treatment decisions and set expectations for recovery or disease progression. In clinical oncology, the valid and prominent question is which radiomics features of radio images are correlated with the prognosis. The answer to this question is solved through the survival analysis which predicts the time to death by establishing a connection between radiomics features and the time to death. The difference of survival analysis from the traditional regression model is that the survival model can work on the partially observed data called censored data. A popular robust mathematical model of survival analysis is Cox proportional hazard model which is expressed in terms of hazard model formula as

$$h(t, X) = h_0(t)e^{\sum_{i=1}^p \beta_i X_i}. \quad (8)$$

That is, Cox survival model is the product of two quantities: $h_0(t)$, baseline hazard function and exponential expression of the linear sum of $\beta_i X_i$ for p radiomics features X_i . Here the hazard means the probability of death. The Cox proportional hazard model does not assume about the distribution for the outcome variable (time to death), but it assumes that the hazard proportion between different subjects is constant over time [8]. The assumption helps to estimate the regression coefficient β_i without considering the full hazard function. This Cox proportional hazard regression model can be used to assess the radiomics features by measuring the predictive discrimination ability [6]. Due to the presence of censored data, this assessment is performed by Concord index (C-index or CI) proposed by Harrell et al in 1982 [6]. The C-index is the measure of how well the patients are sorted according to the event occurrence. The index explains the ability of a radiomics feature to order subjects by estimating the proportion of correctly ordered pairs among all usable pairs in the dataset where the patient pairs have at least one died patient. In our study, as only Lung1 dataset has clinical data having survival time and death status, its four 419 patients are considered to measure the prognostic power through C-index for each feature of 456 radiomics features. In our experiment, 378 RHFMs and 430 wavelet features are above 0.5 and thus show prognostic value. The mean and median CI is approximately 0.54 and 0.55 for both the RHFMs and wavelets, which proves a similar prognostic value.

5 Conclusion and Future Work

We investigated the application of orthogonal moments known as RHFMs for radiomics analysis of lung CT images of NSCLC patients, and compared the extracted RHFMs features with state-of-the-art wavelet features. We proposed a reconstruction framework for RHFMs-based tumour representation, and optimized the feature

selection by the analysis of reconstruction error. Statistical tests were performed to determine the stability, reliability, and prognostic value of the proposed features, which aspects play important roles in clinical oncology. We conclude that orthogonal moments are promising for radiomics analysis, since they show comparable behavior compared to wavelets, while they are more flexible, possibly adaptive, and preferable due to their shift-invariant property. In the future, we plan to further investigate the application of orthogonal moments in radiomics in several respects. This includes the adoption of various orthogonal bases, adaptive transformations, and discretization approaches. We plan to extend the RHF model to 3D, and also direct utilization of transformation invariant moments as radiomic features. Here the feature selection was optimized for the whole databases, but the optimal order is worth to be explored in a patient-wise adaptive manner as well. Furthermore, we will extend our work to build a radiomics signature for associating reliable, stable and prognosis radiomics features and gene expression profiles.

References

- [1] Abu-Mostafa, Y. S. et al. Recognitive Aspects of Moment Invariants. *IEEE Transactions on Pattern Analysis and Machine Intelligence*, PAMI-6(6):698–706, 1984. DOI: [10.1109/TPAMI.1984.4767594](https://doi.org/10.1109/TPAMI.1984.4767594).
- [2] Aerts, H. et al. Decoding tumour phenotype by noninvasive imaging using a quantitative radiomics approach. *Nature Communications*, 5:4006, 2014. DOI: [10.1038/ncomms5006](https://doi.org/10.1038/ncomms5006).
- [3] Chun-peng, W. et al. Geometrically invariant image watermarking based on fast Radial Harmonic Fourier Moments. *Signal Processing: Image Communication*, 45:10–23, 2016. DOI: [10.1016/j.image.2016.03.007](https://doi.org/10.1016/j.image.2016.03.007).
- [4] Coroller, T. P. et al. CT-based radiomic signature predicts distant metastasis in lung adenocarcinoma. *Radiotherapy and Oncology*, 114(3):345–350, 2015. DOI: [10.1016/j.radonc.2015.02.015](https://doi.org/10.1016/j.radonc.2015.02.015).
- [5] Efthymia, N. *Osteoarchaeology: A Guide to the Macroscopic Study of Human Skeletal Remains*. Academic Press, 2016. ISBN: [9780128040973](https://doi.org/9780128040973).
- [6] Harrell, F. E. et al. Evaluating the yield of medical tests. *JAMA*, 247(18):2543–2546, 1982. DOI: [10.1001/jama.1982.03320430047030](https://doi.org/10.1001/jama.1982.03320430047030).
- [7] Hu, M.-K. Visual pattern recognition by moment invariants. *IRE Transactions on Information Theory*, 8(2):179–187, 1962. DOI: [10.1109/TIT.1962.1057692](https://doi.org/10.1109/TIT.1962.1057692).
- [8] Kleinbaum, D. G. et al. *Survival Analysis: A Self-Learning Text*. Statistics for Biology and Health. Springer New York, New York, NY, 2012. DOI: [10.1007/978-1-4419-6646-9](https://doi.org/10.1007/978-1-4419-6646-9).

- [9] Koo, T. K. et al. A Guideline of Selecting and Reporting Intraclass Correlation Coefficients for Reliability Research. *Journal of Chiropractic Medicine*, 15(2):155–163, 2016. DOI: [10.1016/j.jcm.2016.02.012](https://doi.org/10.1016/j.jcm.2016.02.012).
- [10] Lambin, P. et al. Predicting outcomes in radiation oncology–multifactorial decision support systems. *Nature Reviews. Clinical Oncology*, 10(1):27–40, 2013. DOI: [10.1038/nrclinonc.2012.196](https://doi.org/10.1038/nrclinonc.2012.196).
- [11] Li, R. et al. *Radiomics and Radiogenomics: Technical Basis and Clinical Applications*. CRC Press, 2019. ISBN: ISBN: [9780367779580](https://doi.org/10.1007/9780367779580).
- [12] Liu, Y. et al. Accurate quaternion radial harmonic fourier moments for color image reconstruction and object recognition. *Pattern Analysis and Applications*, 23:1–17, 2020. DOI: [10.1007/s10044-020-00877-6](https://doi.org/10.1007/s10044-020-00877-6).
- [13] Pereira, G. C. et al. The Role of Imaging in Radiation Therapy Planning: Past, Present, and Future. *BioMed Research International*, 2014:e231090, 2014. DOI: [10.1155/2014/231090](https://doi.org/10.1155/2014/231090).
- [14] Ping, Z. et al. Image description with Chebyshev–Fourier moments. *JOSA A*, 19(9):1748–1754, 2002. DOI: [10.1364/JOSAA.19.001748](https://doi.org/10.1364/JOSAA.19.001748).
- [15] Prokop, R. J. et al. A survey of moment-based techniques for unoccluded object representation and recognition. *CVGIP: Graphical Models and Image Processing*, 54(5):438–460, 1992. DOI: [10.1016/1049-9652\(92\)90027-U](https://doi.org/10.1016/1049-9652(92)90027-U).
- [16] Ren, H. et al. Multidistortion-invariant image recognition with radial harmonic Fourier moments. *Journal of the Optical Society of America. A, Optics, Image Science, and Vision*, 20(4):631–637, 2003. DOI: [10.1364/josaa.20.000631](https://doi.org/10.1364/josaa.20.000631).
- [17] Sheng, Y. et al. Orthogonal Fourier–Mellin moments for invariant pattern recognition. *Journal of the Optical Society of America A*, 11(6):1748–1757, 1994. DOI: [10.1364/JOSAA.11.001748](https://doi.org/10.1364/JOSAA.11.001748).
- [18] Tang, V. H. et al. Wavelet radiomics features from multiphase CT images for screening hepatocellular carcinoma: Analysis and comparison. *Scientific Reports*, 13(1):19559, 2023. DOI: [10.1038/s41598-023-46695-8](https://doi.org/10.1038/s41598-023-46695-8).
- [19] Teague, M. R. Image analysis via the general theory of moments. *Journal of the Optical Society of America (1917-1983)*, 70:920, 1980. DOI: [10.1364/JOSA.70.000920](https://doi.org/10.1364/JOSA.70.000920).
- [20] Tian, J. et al. *Radiomics and Its Clinical Application: Artificial Intelligence and Medical Big Data*. Academic Press, 2021. ISBN: [978-0-12-818102-7](https://doi.org/10.1016/B978-0-12-818102-7).
- [21] Van Griethuysen, J. J. M. et al. Computational Radiomics System to Decode the Radiographic Phenotype. *Cancer Research*, 77(21):e104–e107, 2017. DOI: [10.1158/0008-5472.CAN-17-0339](https://doi.org/10.1158/0008-5472.CAN-17-0339).

- [22] Zhao, B. et al. Evaluating variability in tumor measurements from same-day repeat CT scans of patients with non-small cell lung cancer. *Radiology*, 252(1):263–272, 2009. DOI: [10.1148/radiol.2522081593](https://doi.org/10.1148/radiol.2522081593).